Force-based Formation Control of Omnidirectional Ground Vehicles

Chiara Gabellieri[1], Alessandro Palleschi, Lucia Pallottino

Abstract— **Formation control of multi-robot systems has been largely studied due to its wide application domain. Several methods in the literature rely on explicit communication among the robots, which in realistic scenarios may lead to reduced performance or even instability due to delays and packet loss or corruption. Nonetheless, multi-robot coordination based solely on implicit communication has been proposed in cooperative manipulation problems. Taking inspiration from this, we propose a method to solve the formation control problem for a group of ground robots not relying on direct communication among them. Instead, the robots are physically constrained to a common object through elastic cables in order to exploit forces as a means of indirect communication. After deriving the dynamic equations, the control and planning approaches are explained, and the stability of the controlled system is discussed using Lyapunov's stability theory. Numerical simulations are presented to support the method.**

I. Introduction

Formation control of multi-robot systems is a classical problem that has received a lot of attention in the literature [1], [2]. Indeed, it is a relevant sub-problem of many applications. Examples are, among others, search and rescue missions, load transport, plant/building management and services, and agriculture use [3]. The basic goals of formation control problems are establishing the formation and keeping it while moving [2].

Formation control approaches have been classified based on the sensing capabilities of the robots and the controlled variables [1]: in *position-based* formations, the controlled variable is the absolute position of each agent; in *displacement-based* formation is the displacement w.r.t. a global reference system; in *distance-based* formation is the relative distance between neighbours.

Formation control approaches have also been grouped, based on the strategy adopted to achieve the sought coordination [2], into *leader-follower*, *virtual structure*, and *behavioral* ones. In *leader-follower* schemes, the followers' primary goal is typically to maintain a desired configuration w.r.t. the leader [4], [5]. The *virtual structure* approach has been introduced in [6] and consists of controlling the robot to maintain certain geometric relations among them, as they were particles of the same rigid body. This approach is generally more fault-tolerant than the leader-follower one and allows precise formation maintenance during trajectory tracking [2]. *Behavioral* formation control has been introduced in [7]. The underlying idea is to generate for each robot a control input that is the weighted sum of different contributions, corresponding to specific formation behaviors, i.e., avoiding static obstacles, avoiding moving obstacles, maintaining the formation, and reaching the target. A theoretical stability proof is difficult for this approach [2].

Robust communication is essential to implement any formation control method [2]. However, communication management inserts some additional complexity into the system, both from a hardware and software point of view, and communication cut-offs and delays in the packet transmission may compromise the performance or even the stability of the formation control in realistic environments and conditions. In general, limitations of the communication range and bandwidth represent an obstacle to large-scale formations [8].

In this work, we propose a formation control approach for multiple omnidirectional vehicles based on an implicit form of communication enabled by force sensing. *Virtual* forces have been widely considered to achieve formation control. Artificial force fields are used to perform obstacle avoidance and converge to the predefined shape [9], [10]. In [11] virtual spring-damper systems are considered between pairs of robots and between each physical robot and a virtual leader robot.

We propose a different approach, in which the robots are connected through physical elastic cables (springs) to a common object. Each robot senses/estimates the force in its own cable. Our idea takes inspiration from our previous work on cooperative force-based manipulation [12], [13], in which robots uniformly distributed on an object regulate its pose. However, in this work, we move the attention from the regulation of the object pose to the control of the robots' formation. The object, physically connected to the robots, is an implicit means of communication among the robots. With our control method, the robots can coordinate themselves in a formation and maintain it while translating, without explicitly sending data to each other. This enables the formation control in environments in which the explicit communication is prevented or disturbed and in situations affected by reduced visibility that would not allow the use of vision-based algorithms. Possible application domains include missions in the presence of dust and fog in the air [14]. Our method leverages a leader-follower scheme in the sense that the leader robot is the only one that possesses some information about the absolute position of the formation, and it controls its own position accordingly. The follower robots, conversely, do not regulate their own position to an

[1] email: chiara.gabellieri1@gmail.com

All the authors are with the Research Center "E. Piaggio" and the Department of Information Engineering of the University of Pisa.

This work has received funding from the Italian Ministry of Education and Research (MIUR) in the framework of the CrossLab project (Departments of Excellence) and from the European Unions Horizon 2020 research and innovation program under agreement no. 732737 (ILIAD).

The authors thank Dr. Riccardo Mengacci for his support in setting up the simulation environment.

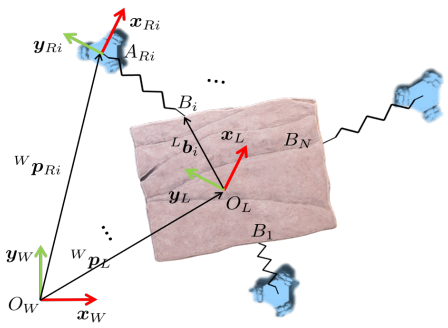


Fig. 1. Schematic representation of the system and its main variables. N omnidirectional ground vehicles with positions ${}^W p_{Ri}$ are connected to a common rigid body with center of mass position ${}^W p_L$ through cables attached at points B_i, which have position ${}^L b_i$ in object frame.

explicit reference value but regulate the force exerted by their own cable. All the robots are controlled with an admittance control law, but the apparent stiffness of the target dynamics of the follower robots is set to zero.

The remainder of the paper is organized as follows. After defining the dynamic equations of the system model in Section II and framing the problem statement in Section III, we propose our control (Section IV) and planning (section V) approaches. The stability of the closed-loop system is proved using Lyapunov's theory. In Section VI, we present the results of simulations validating our method. The conclusions and discussion about future developments are in Section VII.

II. Dynamic Model

In this section, we describe the dynamic model of a group of omnidirectional ground vehicles interconnected through a load by means of elastic elements (see Fig. 1).

Let us first define an inertial frame $\mathscr{F}_W = \{O_W, \boldsymbol{x}_W, \boldsymbol{y}_W, \boldsymbol{z}_W\}$, where $\{\boldsymbol{x}_W, \boldsymbol{y}_W\}$ are its orthogonal unit axes in the horizontal plane and $\boldsymbol{z}_W$ is the vertical axis pointing upward.

We model the manipulated object as a rigid body. We assume that the load has mass $m_L \in \mathbb{R}_{>0}$ and rotational inertia about the vertical axis equal to $j_L \in \mathbb{R}_{>0}$. To describe the state of the load, we define a frame $\mathscr{F}_L = \{O_L, \boldsymbol{x}_L, \boldsymbol{y}_L, \boldsymbol{z}_L\}$ rigidly attached to it and with an origin O_L corresponding to the load center of mass (CoM). We refer to the position and orientation of $\mathscr{F}_L$ with respect to (w.r.t.) $\mathscr{F}_W$ as ${}^W \boldsymbol{p}_L \in \mathbb{R}^2$ and[1] ${}^W \boldsymbol{R}_L \in SO(2)$, which describes a rotation about the vertical axis of an angle ψ. The dependence on ψ is omitted for brevity. We also define as $\dot{\boldsymbol{p}}_L \in \mathbb{R}^2$ and $\boldsymbol{\omega}_L \in \mathbb{R}$ the linear and angular velocity, respectively, of $\mathscr{F}_L$ w.r.t. $\mathscr{F}_W$. The dynamic equations of the rigid body can be simply written as:

$$\begin{aligned} m_L \ddot{\boldsymbol{p}}_L &= \boldsymbol{f}_e \\ j_L \dot{\boldsymbol{\omega}}_L &= \boldsymbol{\tau}_e, \end{aligned} \tag{1}$$

where $\boldsymbol{f}_e \in \mathbb{R}$ is a vector of external forces and $\boldsymbol{\tau}_e$ is the resulting external torque acting on the load CoM. Let us consider in the following that $\boldsymbol{f}_e$ and $\boldsymbol{\tau}_e$ are caused by the forces applied by the cables attached to the rigid body. We refer to the contact point of the i^{th} cable on the load as B_i, with constant position ${}^L \boldsymbol{b}_i \in \mathbb{R}^2$.

We suppose that there are $N > 2$ robots (and hence cables) and that a reference frame, defined as usual as $\mathscr{F}_{Ri} = \{A_i, \boldsymbol{x}_{Ri}, \boldsymbol{y}_{Ri}, \boldsymbol{z}_{Ri}\}$, is attached to the i^{th} robot's CoM. We refer to the position and orientation of $\mathscr{F}_{Ri}$ w.r.t. $\mathscr{F}_W$ as $\boldsymbol{p}_{Ri} \in \mathbb{R}^2$ and $\boldsymbol{R}_{Ri} \in SO(2)$, respectively. The i^{th} robot has mass $m_{Ri} \in \mathbb{R}_{>0}$ and rotational inertia about the vertical axis equal to $j_{Ri} \in \mathbb{R}_{>0}$. We consider omnidirectional vehicles, thus capable of instantaneous movements in any direction on the plane. Each robot is attached to an extensible cable anchored at its CoM through a rotational joint. In this way, the attitude dynamics of the robots is decoupled from the rest of the system dynamics and can be independently controlled at will [12]. Hence, the translational dynamics of the i^{th} robot is written as:

$$m_{Ri} \ddot{\boldsymbol{p}}_{Ri} = -\boldsymbol{f}_i + \boldsymbol{u}_i, \tag{2}$$

where $u \in \mathbb{R}^2$ is the control input and $-\boldsymbol{f}_i \in \mathbb{R}^2$ is the external force acting on the robot. Specifically, we consider the external force due to the cable, and we call $\boldsymbol{f}_i \in \mathbb{R}^2$ the force that the ith cable exerts on the object (its opposite acts on the corresponding robot).

Each cable is modeled as a spring with a rest length $l_{0i} \in \mathbb{R}_{>0}$ and such that

$$\boldsymbol{f}_i = k_i(\|\boldsymbol{l}_i\| - l_{0i}) \frac{\boldsymbol{l}_i}{\|\boldsymbol{l}_i\|} \tag{3}$$

is the elastic force, where $\boldsymbol{l}_i = \boldsymbol{p}_{Ri} - (\boldsymbol{p}_L + \boldsymbol{R}_L {}^L \boldsymbol{b}_i)$ and $k_i \in \mathbb{R}_{>0}$ is the elastic coefficient. In this model, the elastic cable can also push, which is not realistic. However, the model holds when the cable is taut. As it will be more clear in the following, the taut cable assumption is reasonable given the planning and control approaches.

Supposing that the external wrench on the load, composed of $\boldsymbol{f}_e$ and $\boldsymbol{\tau}_e$, is completely due to the cable forces, the dynamics (1) can be written in the following form:

$$\boldsymbol{M}_L \ddot{\boldsymbol{q}}_L = G \boldsymbol{f}, \tag{4}$$

where $\boldsymbol{M}_L = \mathrm{diag}(m_L, j_L)$, $\ddot{\boldsymbol{q}}_L = \begin{bmatrix} \ddot{\boldsymbol{p}}_L^\top & \dot{\boldsymbol{\omega}}_L \end{bmatrix}^\top$, $\boldsymbol{f} \in \mathbb{R}^{2N}$ stacks all the cable forces, and $G \in \mathbb{R}^{3 \times 2N}$ is the grasp matrix. The grasp matrix maps the contact forces, exerted by the cables on the object, to a wrench applied at the object CoM. Specifically, in our case, the grasp matrix can be written as:

$$G = \begin{bmatrix} \boldsymbol{I}_2 & \cdots & \boldsymbol{I}_2 \\ \boldsymbol{R}_L S_2({}^L \boldsymbol{b}_1) & \cdots & \boldsymbol{R}_L S_2({}^L \boldsymbol{b}_N) \end{bmatrix}, \tag{5}$$

with $\boldsymbol{I}_i \in \mathbb{R}^{i \times i}$ the identity matrix of dimension i, and S_2 the analog of the cross-product matrix (the analog of the skew operator) for two-dimensional vector, given as: $S_2(\begin{bmatrix} a_x & a_y \end{bmatrix}) := \begin{bmatrix} -a_y & a_x \end{bmatrix}^\top$ [15].

III. Problem Statement

Our problem can be formulated as follows. Given a set of points A_i, with positions $\boldsymbol{p}_{Ai}$, describing the desired formation

[1]The left superscript indicates the reference frame. From now on, $\mathscr{F}_W$ is considered as the reference frame when the superscript is omitted.

of the robots, and an object with its frame $\mathscr{F}_L$, we want to bring the robots in the formation and to maintain the formation without leveraging direct data exchange. To do so, we physically connect the robots to the common object through cables. The cable anchoring points on the object, B_i, are free parameters to be set. Note that the shape of the considered object is irrelevant since we can anyway model the object dynamics considering solely its CoM and the points B_i.

To comply with the desired formation, the kinematics of the system imposes that

$$\boldsymbol{p}_{Ri} = \boldsymbol{p}_{Ai} = \boldsymbol{p}_L + \boldsymbol{b}_i + l_0 \frac{\boldsymbol{f}_i}{\|\boldsymbol{f}_i\|} + \frac{\boldsymbol{f}_i}{k_i} \tag{6}$$

for a certain value of the i^{th} cable force, $\boldsymbol{f}_i$. These forces should be of equilibrium for the object in order to maintain the formation, i.e., we impose:

$$G\boldsymbol{f} = 0. \tag{7}$$

We need to find a suitable control law and a method to plan the control references to achieve the aforementioned objectives.

IV. Control

In order to reach the formation and translate it without relying on explicit communication, we propose to use admittance control. First, following standard implementation of the admittance controller, we suppose that each robot implements a trajectory tracking control law and is thus capable of following the desired trajectory, ideally with no error. In other words, this will be achieved using u_i in (2). Hence, we assign to each robot a reference trajectory consisting of the state of the following admittance filter:

$$\boldsymbol{M}_{Ai}(\ddot{\boldsymbol{p}}^r_{Ri} - \ddot{\boldsymbol{p}}^d_{Ri}) + \boldsymbol{B}_{Ai}(\dot{\boldsymbol{p}}^r_{Ri} - \dot{\boldsymbol{p}}^d_{Ri}) + \boldsymbol{K}_{Ai}(\boldsymbol{p}^r_{Ri} - \boldsymbol{p}^d_{Ri}) = \boldsymbol{f}^d_i - \boldsymbol{f}_i, \tag{8}$$

where $(\cdot)^r$ indicates the state of the system and $(\cdot)^d$ the corresponding desired references. $\boldsymbol{M}_{Ai}$, $\boldsymbol{B}_{Ai}$, and $\boldsymbol{K}_{Ai}$, all $\in \mathbb{R}^{2\times 2}$, are the desired inertia, damping, and stiffness matrices, respectively, and represent tunable control gains. Basically, if the trajectory tracking is perfect, the system exactly replicates the motion of the dynamic system in (8), subject to an external force equal to $\boldsymbol{f}^d_i - \boldsymbol{f}_i$. Indeed, the objective of the admittance control is that of reshaping the dynamic behavior of the robot so that it responds by changing its trajectory in the desired way when perturbed by an external force. In the following, similar to [12], [13], we will suppose perfect tracking and thus we will consider the dynamics of each robot to be coincident to (8), where $\boldsymbol{p}^r_{Ri} = \boldsymbol{p}_{Ri}$, and so on. Hence, we obtain the closed-loop dynamics of each robot:

$$\boldsymbol{M}_{Ai}(\ddot{\boldsymbol{p}}_{Ri} - \ddot{\boldsymbol{p}}^d_{Ri}) + \boldsymbol{B}_{Ai}(\dot{\boldsymbol{p}}_{Ri} - \dot{\boldsymbol{p}}^d_{Ri}) + \boldsymbol{K}_{Ai}(\boldsymbol{p}_{Ri} - \boldsymbol{p}^d_{Ri}) = \boldsymbol{f}^d_i - \boldsymbol{f}_i. \tag{9}$$

Note that, even though the simplifying assumption of perfect trajectory tracking is made for the theoretical analysis, the simulations are carried out disregarding such an assumption in order to validate the algorithm in a more realistic scenario. Note also that the controller implementation requires that each robot senses or estimates the external force acting through its own cable. For the sake of clarity, the control scheme is reported in figure 2. Once we have chosen the control gains $\boldsymbol{M}_{Ai}$, $\boldsymbol{B}_{Ai}$, and $\boldsymbol{K}_{Ai}$ according to a desirable dynamic behavior of the vehicles, e.g., critically damped or over-damped, it remains open how to chose the references, $\boldsymbol{f}^d_i$ and $\boldsymbol{p}^d_{Ri}$, in order to achieve our control goal.

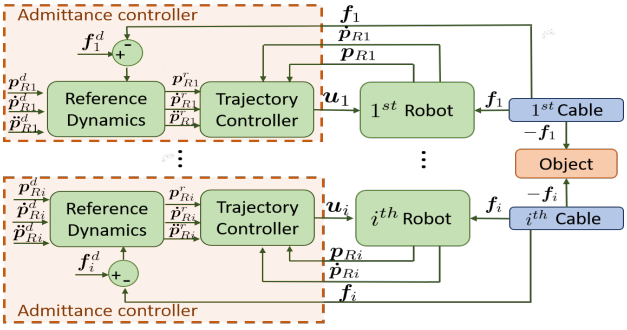


Fig. 2. The admittance controller implementation consists of simulating a reference dynamics with desired motion labeled by the superscript $(\cdot)^d$ and characterized by the state indicated with $(\cdot)^r$. This is fed into a trajectory controller—with higher bandwidth than that of the dynamic compliant frame—as a reference input. There is a reference force $\boldsymbol{f}^d_i$, so that a dynamic response is induced in the compliant frame if $\boldsymbol{f}_i \neq \boldsymbol{f}^d_i$.

We propose to leverage a leader-follower scheme. Without loss of generality, we assume that robot 1 is the leader robot. The fundamental step is to set, $\forall i > 1$, $\boldsymbol{K}_{Ai} = \boldsymbol{0}_{2\times 2}$. On the contrary, an apparent stiffness different from zero is chosen for the leader robot. This means that the leader robot is the only one to be attracted to a reference position. The follower robots, conversely, tend to stay where they are if not perturbed by the external forces. If the value of the external force changes w.r.t. the reference, $\boldsymbol{f}^d_i$, the follower robots move to restore the desired value of the external force. Furthermore, all the robots contribute to damping possible oscillations. Basically, when the leader robot moves towards its reference position, it drags the common object through its cable and thus the cables of the follower robots are pulled, too. The follower robots, in response to the change of the cable forces, move to restore the reference values, following the leader robot motion as a result. A similar approach has been also exploited, e.g., in [16] with two aerial vehicles, and [17] for a human leader and an aerial vehicle serving as the follower.

V. Planning

In this section, we explain how we pick the reference values of the external force for each robot, and the reference position for the leader robot in order to achieve the sought formation. We propose to solve an off-line constrained optimization problem to find the robots' reference forces and the cable anchoring points on the load. Leveraging the results from grasp planning theory [18], we set the cost function equal to the maximum of the contact-force intensities. In this way, while decreasing the stress imposed on the object and on the robot themselves, we reduce the control effort required to perform the formation task and distribute the effort among the robots.

Equations (6) and (7) represent equality constraints of the aforementioned optimization problem. The contact forces that result from solving (7) can be parametrized according to a certain base of the nullspace of G, call it E:

$$\boldsymbol{f} = E\boldsymbol{\lambda}, \tag{10}$$

where vector $\boldsymbol{\lambda}$, with components λ_i, is used to parametrize the *internal force* in the basis E. Its importance has been highlighted in the literature of robotic grasping—see, e.g., [15]. As it will be more clear in the following, the internal forces are a crucial element of our formation control law. We conveniently write down (10) exploiting a particular base of the nullspace of G. In fact, the internal forces can be expressed as couples of equal and opposite forces applied at two contact points and acting along the line that connects the points [19]. In the following, we report (10) for the three-robot case:

$$\boldsymbol{f} = \begin{bmatrix} \boldsymbol{e}_{1,2} & \boldsymbol{0}_{2\times 1} & \boldsymbol{e}_{1,3} \\ -\boldsymbol{e}_{2,1} & \boldsymbol{e}_{2,3} & \boldsymbol{0}_{2\times 1} \\ \boldsymbol{0}_{2\times 1} & -\boldsymbol{e}_{2,3} & -\boldsymbol{e}_{1,3} \end{bmatrix} \begin{bmatrix} \lambda_1 \\ \lambda_2 \\ \lambda_3 \end{bmatrix} \tag{11}$$

with $\boldsymbol{e}_{i,j} \in \mathbb{R}^2$ the unit vector along the direction B_jB_i. Formally,

$$\boldsymbol{e}_{i,j} = \frac{{}^L\boldsymbol{b}_i - {}^L\boldsymbol{b}_j}{||{}^L\boldsymbol{b}_i - {}^L\boldsymbol{b}_j||}. \tag{12}$$

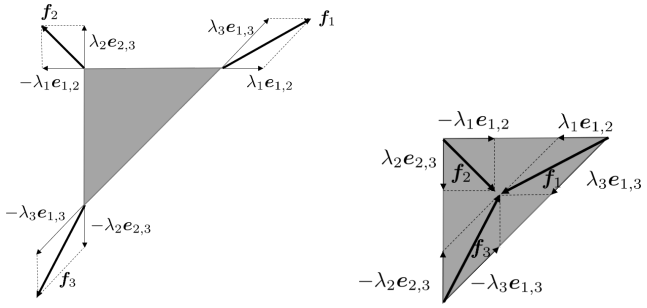
Refer to Fig. 3 for a schematic representation. For more than three robots, matrix E can be written in an analogous way [19].

Eventually, we can write:

$$\begin{aligned} \min_{\boldsymbol{b}_i, \boldsymbol{f}_i, \lambda_i} \quad & \max(||{}^L\boldsymbol{f}_i||) \\ \text{s.t.} \quad & {}^L\boldsymbol{f}_i = E(i,:)\boldsymbol{\lambda} \\ & {}^L\boldsymbol{p}_{Ai} = {}^L\boldsymbol{b}_i + l_0\,{}^L\boldsymbol{f}_i/||{}^L\boldsymbol{f}_i|| + {}^L\boldsymbol{f}_i/K_c \\ & \lambda_i \geq \gamma_i, \end{aligned} \tag{13}$$

where $\gamma_i > 0$ is a defined threshold. By solving problem (13), we find a set of cable anchoring points on the load and cable forces, ${}^L\bar{\boldsymbol{b}}i$ and $\bar{\boldsymbol{f}}_i$, respectively, such that the robots are in the desired formation given by the positions $\boldsymbol{p}_{Ai}$ and the load is at equilibrium. We call the equilibrium rotation matrix of the object $\bar{\boldsymbol{R}}_L$. It corresponds to $\bar{\psi}$ and is such that $\sum_{i=1}^N \bar{\boldsymbol{R}}_L S_2({}^L\bar{\boldsymbol{b}}_i)\bar{\boldsymbol{f}}_i = \boldsymbol{0}$. From easy computations using (11), (12), and trigonometric relations, one finds that there is another value $\psi = \bar{\psi} \pm \pi$ for which the previous relation is verified. This rotated configuration, however, corresponds to forces that push the object, and, as we will see, is unstable. Note that, having chosen $\lambda_i > 0$, the reference cable forces stretch the object and the assumption of taut cables is realistic. Moreover, one can choose the value of λ_i based on the robustness of the object and robots available (e.g., high stresses may tear apart a fragile object).

Proposition Setting the robots' references in (8) as $\boldsymbol{p}^d_{R1} = \boldsymbol{p}_{A1}$ and $\boldsymbol{f}^d_i = \bar{\boldsymbol{f}}_i$ and attaching the cables on the load such that ${}^L\boldsymbol{b}_i = {}^L\bar{\boldsymbol{b}}_i$, provided that $\forall i = 1,...,N\ \lambda_i > 0$, the robots converge to the desired formation.



(a) $\lambda_i > 0$ (b) $\lambda_i < 0$

Fig. 3. Representation of a distribution of internal forces on the same object changing the sign of the parameters λ_i. The generation of the internal forces as couples of equal and opposite forces acting on the connections of the contact points is highlighted.

Proof. We will first show that the desired formation is an equilibrium of the system under the aforementioned control references. Hence, we will show that the equilibrium is asymptotically stable. Let us derive the conditions of equilibrium for the closed-loop system by imposing constantly zero velocities in (9) and (4). By doing so, we obtain the following system of equations:

$$\begin{cases} \boldsymbol{K}_{A1}(\boldsymbol{p}_{R1} - \boldsymbol{p}^d_{R1}) = \boldsymbol{f}^d_1 - \boldsymbol{f}_1 & \text{(14a)} \\ 0 = \boldsymbol{f}^d_i - \boldsymbol{f}_i,\ \forall i > 1 & \text{(14b)} \\ 0 = \sum_{i=1}^N \boldsymbol{f}_i & \text{(14c)} \\ 0 = \sum_{i=1}^N \boldsymbol{R}_L S_2({}^L\boldsymbol{b}_i)\boldsymbol{f}_i. & \text{(14d)} \end{cases}$$

From the first three equations, we obtain that, $\forall i = 1,...,N$, $\boldsymbol{f}_i = \boldsymbol{f}^d_i = \bar{\boldsymbol{f}}_i$ and that $\boldsymbol{p}_{R1} = \boldsymbol{p}^d_{R1} = \boldsymbol{p}_{A1}$, as desired. Provided that $\lambda_i \neq \boldsymbol{0}$, and hence that $\bar{\boldsymbol{f}}_i$ is different from zero, (14d) becomes $0 = \sum_{i=1}^N \boldsymbol{R}_L S_2({}^L\bar{\boldsymbol{b}}_i)\bar{\boldsymbol{f}}_i$, which is true for $\boldsymbol{R}_L = \bar{\boldsymbol{R}}_L$. Being ${}^L\boldsymbol{b}_i = {}^L\bar{\boldsymbol{b}}_i$, $\boldsymbol{p}_{R1} = \boldsymbol{p}_{A1}$, $\boldsymbol{R}_L = \bar{\boldsymbol{R}}_L$, and $\boldsymbol{f}_i = \bar{\boldsymbol{f}}_i$, we have that, $\forall i = 1,...,N$, $\boldsymbol{p}_{Ri} = \boldsymbol{p}_{Ai}$ by construction.

We showed that, with the given control references and cable anchoring points on the object, the desired formation is an equilibrium of the closed-loop system. We define now the vector $\boldsymbol{q}_R \in \mathbb{R}_{2N}$ that stacks all the robot positions. Calling $\boldsymbol{q} = \begin{bmatrix} \boldsymbol{q}_R^\top & \boldsymbol{q}_L^\top \end{bmatrix}^\top$, and provided that ${}^L\boldsymbol{b}_i = {}^L\bar{\boldsymbol{b}}_i$, we define $\bar{\boldsymbol{q}} = \{\boldsymbol{q} : \boldsymbol{p}_{R1} = \boldsymbol{p}_{A1}, \boldsymbol{f}_i = \bar{\boldsymbol{f}}_i, \boldsymbol{R}_L = \bar{\boldsymbol{R}}_L\}$, and $\boldsymbol{x} = (\boldsymbol{q}, \dot{\boldsymbol{q}})$ as the state of the system. In the following, we will show that, if $\lambda_i > 0$, the equilibrium state $\bar{\boldsymbol{x}} = (\bar{\boldsymbol{q}}, \boldsymbol{0})$ is asymptotically stable.

We define vector $\boldsymbol{e}_{Ri} = \boldsymbol{p}_{Ri} - \boldsymbol{p}^d_{Ri}$ as the leader position error. Similar to [13], which faced pose regulation of the object with the robots *uniformly* distributed around its CoM, let us consider the following function:

$$\begin{aligned} \hat{V}(\boldsymbol{x}) = & \frac{1}{2}\Big[\sum_{i=1}^N \Big(\dot{\boldsymbol{p}}_{Ri}^\top \boldsymbol{M}_{Ai}\dot{\boldsymbol{p}}_{Ri} + \boldsymbol{e}_{Ri}^\top \boldsymbol{K}_{Ai}\boldsymbol{e}_{Ri}\Big) + \dot{\boldsymbol{p}}_L{}^\top \boldsymbol{M}_L\dot{\boldsymbol{p}}_L + \\ & + \boldsymbol{\omega}_L^\top J_L\boldsymbol{\omega}_L + \sum_{i=1}^N k_i((\|\boldsymbol{l}_i\| - l_{0i})^2 - 2\boldsymbol{l}_i^\top \bar{\boldsymbol{f}}_i\Big] + \\ & + \sum_{i=1}^N \bar{\boldsymbol{f}}_i^\top \bar{\boldsymbol{R}}_L{}^L\bar{\boldsymbol{b}}_i - \sum_{i=1}^N \bar{\boldsymbol{f}}_i^\top \boldsymbol{R}_L{}^L\bar{\boldsymbol{b}}_i. \end{aligned} \tag{15}$$

First, we want to show that

$$V(\boldsymbol{x}) = \hat{V}(\boldsymbol{x}) - \hat{V}(\bar{\boldsymbol{x}}) \tag{16}$$

is a candidate Lyapunov function, namely:

i) $\boldsymbol{x}_{\min} = \operatorname{argmin}_{\boldsymbol{x}} \hat{V}(\boldsymbol{x})$ is such that $\boldsymbol{x}_{\min} = \bar{\boldsymbol{x}}$ if, $\forall i = 1,\dots,N,\ \lambda_i > 0$;

ii) $V(\boldsymbol{x})$ is positive definite in a neighbourhood of $\bar{\boldsymbol{x}}$.

We split (16) into three parts such that

$$\hat{V}(\boldsymbol{x}) = \bar{V}(\boldsymbol{x}) + \sum V_i'(\boldsymbol{x}) + \sum \tilde{V}_i(\boldsymbol{x}), \tag{17}$$

where

$$\bar{V}(\boldsymbol{x}) = \frac{1}{2}\sum_{i=1}^{N}\left(\dot{\boldsymbol{p}}_{Ri}^{\top}\boldsymbol{M}_{Ai}\dot{\boldsymbol{p}}_{Ri} + \boldsymbol{e}_{Ri}^{\top}\boldsymbol{K}_{Ai}\boldsymbol{e}_{Ri}\right) + \dot{\boldsymbol{p}}_L{}^{\top}\boldsymbol{M}_L\dot{\boldsymbol{p}}_L + + \boldsymbol{\omega}_L^{\top} j_L \boldsymbol{\omega}_L \tag{17a}$$

$$V_i'(\boldsymbol{x}) = \frac{1}{2}k_i(\|\boldsymbol{l}_i\| - l_{0i})^2 - \boldsymbol{l}_i^{\top}\bar{\boldsymbol{f}}_i \tag{17b}$$

$$\tilde{V}(\boldsymbol{x}) = \bar{\boldsymbol{f}}_i^{\top}\bar{\boldsymbol{R}}_L{}^{L}\bar{\boldsymbol{b}}_i - \bar{\boldsymbol{f}}_i^{\top}\boldsymbol{R}_L{}^{L}\bar{\boldsymbol{b}}_i. \tag{17c}$$

We shall show that all the terms that compose $\hat{V}(\boldsymbol{x})$ have a minimum in $\bar{\boldsymbol{x}}$.

This clearly holds for the quadratic terms in (17a). Also, it has been shown in [12] that $V_i'(\boldsymbol{x})$ is radially unbounded, i.e., $\lim_{\|\boldsymbol{x}\|\to\infty} V_i'(\boldsymbol{x}) = \infty$. Based on this result and on Theorem 1.15 of [20], function (17) has a global minimum. It has been shown in [12] that the global minimum of (17) is in $\bar{\boldsymbol{x}}$. Eventually, in order to prove point i), in this case, we also need to show that $\tilde{V}(\boldsymbol{x})$ has a minimum in $\boldsymbol{x} = \bar{\boldsymbol{x}}$. The proof of this point is provided in the Appendix.

Thus, we have that $V(\boldsymbol{x})$ in (16) is such that $V(\boldsymbol{x}) = 0$ if $\boldsymbol{x} = \bar{\boldsymbol{x}}$ and $V(\boldsymbol{x}) > 0$ otherwise, proving points i) and ii).

Let us now compute the time derivative of (16):

$$\dot{V}(\boldsymbol{x}) = \sum_{i=1}^{N}\left(\dot{\boldsymbol{p}}_{Ri}^{\top}\boldsymbol{M}_{Ai}\ddot{\boldsymbol{p}}_{Ri} + \boldsymbol{e}_{Ri}^{\top}\boldsymbol{K}_{Ai}\dot{\boldsymbol{e}}_{Ri} + \dot{\boldsymbol{l}}_i^{\top}\boldsymbol{f}_i - \dot{\boldsymbol{l}}_i^{\top}\bar{\boldsymbol{f}}_i + - \bar{\boldsymbol{f}}_i^{\top}\boldsymbol{S}(\boldsymbol{\omega}_L)\boldsymbol{R}_L{}^{L}\bar{\boldsymbol{b}}_i\right) + m_L\dot{\boldsymbol{p}}_L^{\top}\ddot{\boldsymbol{p}}_L + \boldsymbol{\omega}_L^{\top} j_L\dot{\boldsymbol{\omega}}_L, \tag{18}$$

where we used the fact that $\frac{d}{dt}\left(\frac{1}{2}k_i(\|\boldsymbol{l}_i\| - l_{0i})^2\right) = \dot{\boldsymbol{l}}_i^{\top}\boldsymbol{f}_i$.

Substituting (9) and (4) and noting that $\dot{\boldsymbol{l}}_i = \dot{\boldsymbol{p}}_{Ri} - \dot{\boldsymbol{p}}_L - \boldsymbol{S}(\boldsymbol{\omega}_L)\boldsymbol{R}_L{}^{L}\boldsymbol{b}_i$, after few algebraic computations we get:

$$\dot{V}(\boldsymbol{x}) = \sum_{i=1}^{N} -\dot{\boldsymbol{p}}_{Ri}^{\top}\boldsymbol{B}_{Ai}\dot{\boldsymbol{p}}_{Ri}, \tag{19}$$

which is clearly negative semidefinite. By substituting $\hat{\boldsymbol{x}} = \{\boldsymbol{x} : \dot{V}(\boldsymbol{x}) \equiv 0\}$ into (9) and (4), one can easily find that $\bar{\boldsymbol{x}}$ in an invariant set. In fact, $\boldsymbol{p}_{Ri} = \text{const}$ brings to (14a) and (14b). Then, since all quantities in (14a) and (14b) must be constant, it is not possible for the load to have $\dot{\boldsymbol{\omega}}_L \neq 0$ or $\ddot{\boldsymbol{p}}_L \neq 0$ in (4). From these considerations, one obtains (14c) and (14d) with $\boldsymbol{f}_i = \bar{\boldsymbol{f}}_i$, which bring to $\boldsymbol{x} = \bar{\boldsymbol{x}}$. Consequently, we conclude for La Salle's invariance principle that, if $\lambda_i > 0$, $\bar{\boldsymbol{x}}$ is locally stable. □

Considerations on the internal forces λ_i: One could think of choosing $\lambda_i = 0$, thus avoiding internal stress in the object and additional control effort required to generate the internal force. However, this choice would not be convenient for our purpose. In fact, in that case, (14d) would be verified for every $\boldsymbol{R}_L$. The desired formation is still an equilibrium of the closed-loop system under the reference inputs, but it belongs to a *continuum* of equilibrium points and hence it is *marginally* but not *asymptotically* stable. In particular, while at the equilibrium the leader robot is in its desired position, the positions of the follower robots, correspond to their reference forces, are arbitrary and the formation may not be reached.

Instead, choosing $\lambda_i < 0$ would be unfeasible in practice for a ground system like the one we are considering since the cables should push the object or cross it (see Fig. 3(b)). However, as it will be shown by the simulation results in Section VI, this choice would lead to the formation being an unstable equilibrium for the system. Similar conclusions have been drawn, e.g., in [13] for the particular case of vehicles uniformly distributed around the object CoM.



Fig. 4. Three omnidirectional vehicles simulated in the Gazebo dynamic simulator.

	$i = 1$	$i \neq 1$
$\boldsymbol{M}_{Ai}$ (kg)	$0.5\boldsymbol{I}_2$	$0.01\boldsymbol{I}_2$
$\boldsymbol{B}_{Ai}$ (kg·m^{-1})	$0.5\boldsymbol{I}_2$	$0.01\boldsymbol{I}_2$
$\boldsymbol{K}_{Ai}$ (kg·m^{-2})	$1000\boldsymbol{I}_2$	$0\boldsymbol{I}_2$
$K_P = 0.5$, $K_I = 0.1\text{s}^{-1}$, $m_L = 0.5\text{kg}$, $j_L = 1\text{kg}\cdot\text{m}^2$ $l_{0i} = 0.5\text{m}$, $k_i = 10\ \text{kg}\cdot\text{m}^{-2}$		

TABLE I

SIMULATION PARAMETERS

VI. SIMULATIONS

In this section, we provide the results of numerical simulations to validate our method. The simulations have been carried out in MATLAB Simulink and ROS Gazebo. The offline optimization problem to plan the references has been solved using the optimization software CasADi [21] in Matlab. The load and elastic cables, the admittance reference dynamic system, and the leader robot trajectory generation run in MATLAB Simulink. Three-wheeled omnidirectional vehicles have been simulated in Gazebo as shown in Fig. 4. The robots are controlled with a velocity PI controller on each wheel, with constant gains K_P and K_I. The code for one vehicle was available on GitHub[2] and has been modified in this work to handle multi-robot simulations. The robots receive the output of the admittance filter through Simulink-ROS communication interface. The forces that act on the object and on the robots are also sent to Gazebo and applied to the vehicles. The positions of the vehicles computed in Gazebo are sent back to Simulink and used in the admittance filters and in the cable dynamics. The main parameters of the simulations are reported in Table I.

[2] https://github.com/GuiRitter/OpenBase

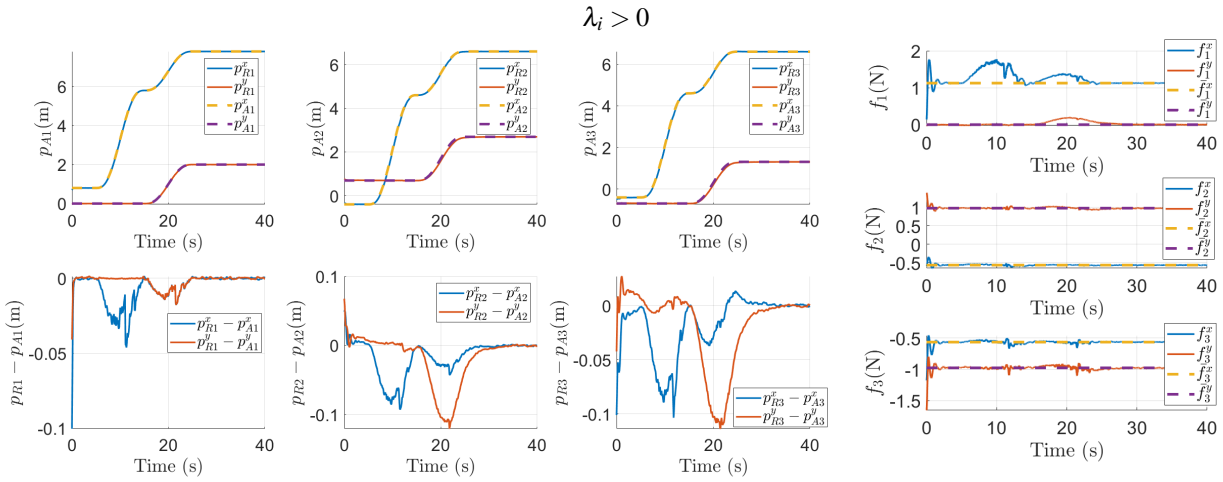


Fig. 5. Results of the simulation for $\lambda_i > 0$ ($\gamma_i = 2$). On the left, the evolution of $\boldsymbol{p}_{Ri}$ and its error w.r.t the corresponding position on the desired formation, $\boldsymbol{p}_{Ai}$. On the right, the evolution of $\boldsymbol{f}_i$. The robots converge to the desired formation. Note that only the leader robot is attracted to a desired position, while the other robots follow the desired position indirectly, by regulating the external force in the cable through the admittance controller.

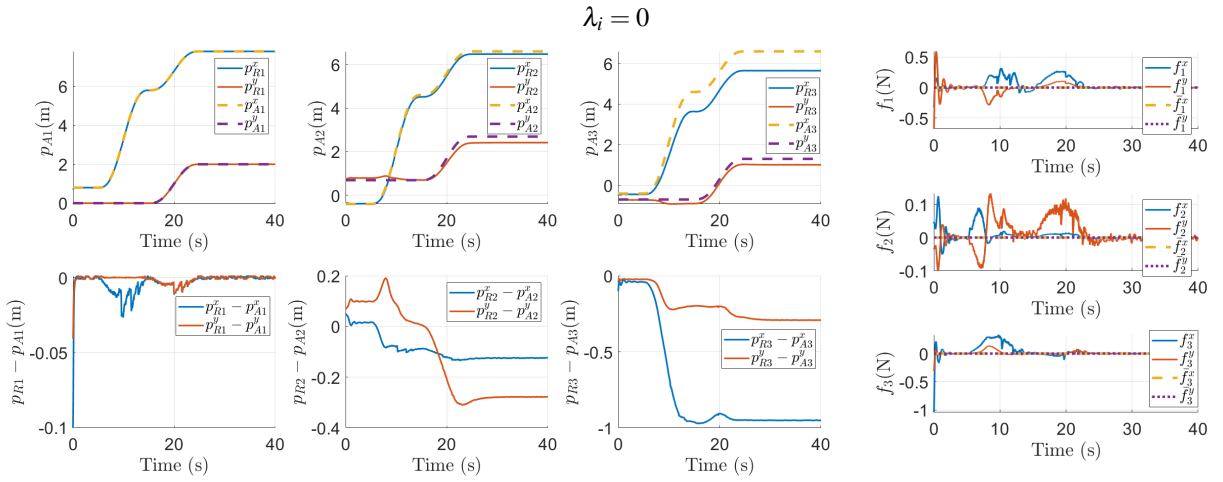


Fig. 6. Results of the simulation for $\lambda_i = 0$. On the left, the evolution of $\boldsymbol{p}_{Ri}$ and its error w.r.t the corresponding position on the desired formation, $\boldsymbol{p}_{Ai}$. On the right, the evolution of $\boldsymbol{f}_i$. The robots do not converge to the desired formation. They assume a different formation that is not unique but depends on the initial conditions and the trajectory of the leader robot.

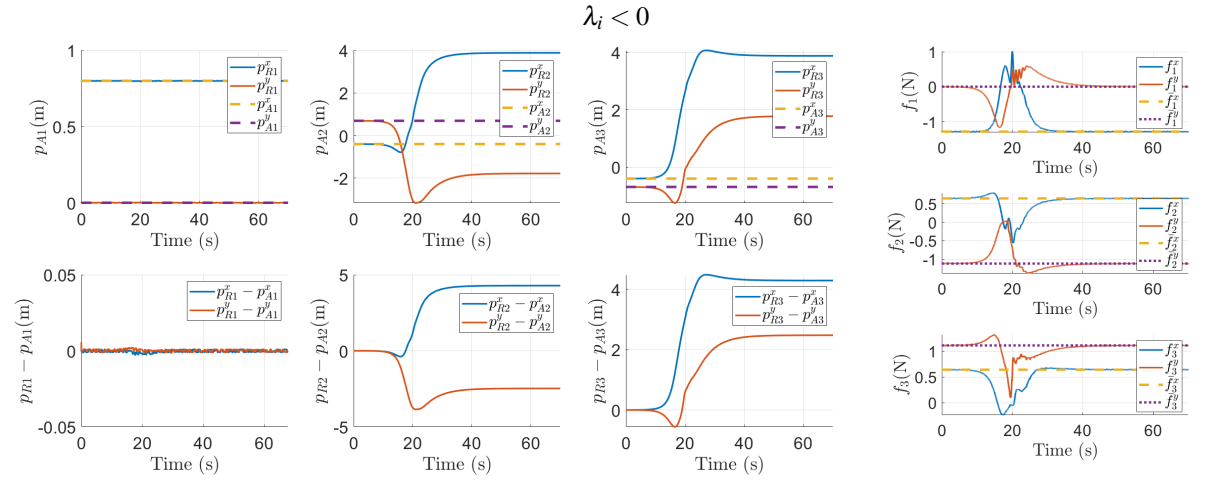


Fig. 7. Results of the simulation for $\lambda_i < 0$. On the left, the evolution of $\boldsymbol{p}_{Ri}$ and its error w.r.t the corresponding position on the desired formation, $\boldsymbol{p}_{Ai}$. On the right, the evolution of $\boldsymbol{f}_i$. The robots diverge from the desired formation despite being initialized already in the desired positions. They converge to a different formation in which the cables stretch the load—an asymptotically stable configuration for what has been said.

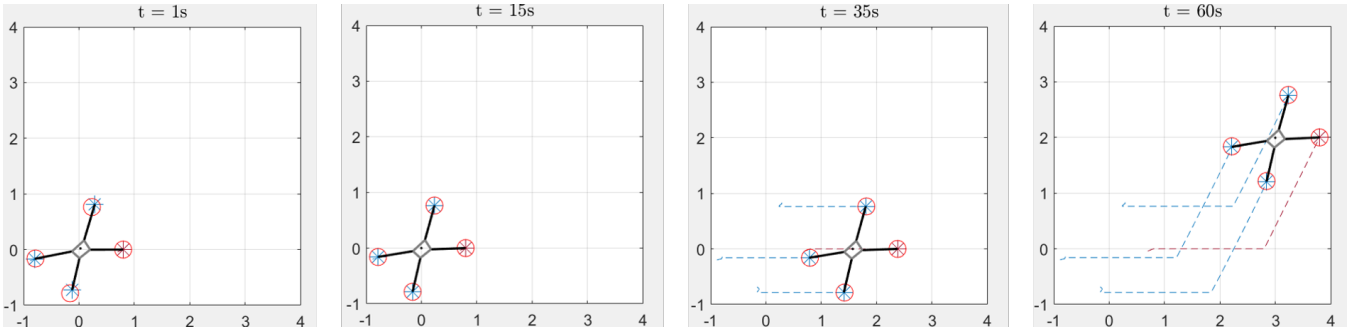


Fig. 8. Visualization of a system of four vehicles, where the axis are in meters. The vehicles are represented as stars, the red one is the leader. The red circles are the positions in the desired formation. The cables are black lines, and the grey lines connect the cable anchoring points on the load. The dashed lines are the past trajectories of the robots (red for the leader). $\lambda_i > 0$, so the robots establish the desired formation (second frame) even though there are not initialized in it (first frame). The trajectory is piece-wise polynomial (see the last two frames). For the first 25 seconds, the desired formation remains the same. Then, the leader robot must move of 2 meters along $\boldsymbol{x}_W$ for 15 seconds, and of 1 meter along $\boldsymbol{x}_W$ and 2 meters along $\boldsymbol{y}_W$ for the last 20 seconds.

First, we show the results of two simulations, one in which $\lambda_i > 0$ (Fig.5) and one in which $\lambda_i = 0$ (Fig. 6). Since the method has been derived for steady-state convergence, in order for the formation to follow a reference motion accurately, it must be sufficiently slow. By tuning the admittance filter gains, however, the user changes the dynamic response of the robots, and hence the responsiveness of the followers. We set a 5^{th}-order piece-wise polynomial trajectory. Each piece of the trajectory starts and ends with zero velocity and zero acceleration. The desired initial formation is given by $\boldsymbol{p}_{A1} = \begin{bmatrix} 0.8000 & 0 \end{bmatrix}^\top$ m, $\boldsymbol{p}_{A2} = \begin{bmatrix} -0.4000 & 0.6928 \end{bmatrix}^\top$, $\boldsymbol{p}_{A3} = \begin{bmatrix} -0.4000 & -0.6928 \end{bmatrix}^\top$ m. The robots' initial positions, $\boldsymbol{p}_{Ri}(0)$ do not coincide with the desired formation. Specifically, $\boldsymbol{p}_{R1}(0) = \begin{bmatrix} 0.7000 & -0.0400 \end{bmatrix}^\top$ m, $\boldsymbol{p}_{R2}(0) = \begin{bmatrix} -0.3500 & 0.7628 \end{bmatrix}^\top$ m, and $\boldsymbol{p}_{R3}(0) = \begin{bmatrix} -0.5000 & -0.7328 \end{bmatrix}^\top$ m. For the first 5 seconds, the leader is commanded to go to $\boldsymbol{p}_{A1}$ and the robots' goal is to establish the formation. Then, the formation is commanded (through the leader's desired trajectory) to translate of 5 meters along $\boldsymbol{x}_W$ in 10s and then of 2 meter along $\boldsymbol{y}_W$ and 2 meters along $\boldsymbol{z}_W$ in the following 10 seconds. When $\lambda_i > 0$, the robots reach the desired formation and move maintaining it—see Fig. 5. When $\lambda_i = 0$, instead, the follower robots are not capable of bringing themselves to the desired formation—see Fig. 6. They assume different configurations depending on the initial conditions and the motion of the leader robot.

Note that $\lambda_i < 0$, for a planar system as the one we are considering, leads to a setup that is not feasible in practice because the cables should push the load or cross it. However, it is possible to simulate numerically the behavior of the system. In Fig. 7, we report the simulation results when $\lambda_i < 0$, showing that the desired formation is an unstable equilibrium of the system. Indeed, in this case, the robots are initialized in the desired formation and the leader is commanded to stay in $\boldsymbol{p}_{A1}$ for all the duration of the simulation. However, the robots diverge from the desired and initial formation, converging to a different one in which $\boldsymbol{p}_{R1} = \boldsymbol{p}_{A1}$ as commanded, but the cable forces *stretch* the object. A similar result had been obtained in the different context of cooperative manipulation in [13].

In Fig. 8, the reader can appreciate a visualization of the evolution of a system composed of four robots and $\lambda_i > 0$.

VII. Conclusions and Future Work

This paper proposes a novel method for bringing to and maintaining in a desired formation a group of physically constrained omnidirectional ground vehicles that do not exchange any data. The admittance-controlled robots are attached with elastic cables to a common load, which serves as a means of implicit communication among them. They use the force in their own cable to achieve the sought coordination thanks to a leader-follower scheme. This enables the formation control in environments in which the explicit communication is prevented or disturbed, and avoids all issues related to communication delays and packet loss. The stability of the controlled system is proven using Lyapunov-based techniques, and simulations using ROS Gazebo and MATLAB Simulink are reported to validate the proposed approach.

Further studies will be conducted to assess additional capabilities of the group of robots, i.e., the rotation of the overall formation around its geometric center and the scaling of the formation, which may be particularly useful for obstacle avoidance. However, the cables may impede the motion of the formation in clutter environments, and their extension range set a bound to the feasible scale factors of the formation. The extension of the proposed method to aerial robots will be investigated. Underwater robotics, typically affected by communication issues, might open to interesting applications. Experiments on hardware vehicles will be carried out as a crucial test bed to appreciate the performance of the proposed method.

Appendix

In this section, we are going to show that, for $\lambda_i > 0$,

$$\tilde{V}(\boldsymbol{x}) > 0, \ \forall \boldsymbol{x} \neq \bar{\boldsymbol{x}}. \tag{20}$$

Note that $\tilde{V}(\bar{\boldsymbol{x}}) = 0$. We write (20) in the expanded form

$$\sum_{i=1}^{N} \bar{\boldsymbol{f}}_i^{\top} \bar{\boldsymbol{R}}_L {}^L\boldsymbol{b}_i - \sum_{i=1}^{N} \bar{\boldsymbol{f}}_i^{\top} \boldsymbol{R}_L {}^L\boldsymbol{b}_i > 0, \ \forall \boldsymbol{x} \neq \bar{\boldsymbol{x}}. \tag{21}$$

In the following, we will assume that ${}^L\boldsymbol{b}_i = {}^L\bar{\boldsymbol{b}}_i$, namely we suppose to have attached the cables to the load in the desired way. Consider for now $N = 3$. Remember that, according to (10), we can write

$$\begin{cases} \bar{\boldsymbol{f}}_1 = +\lambda_1 \frac{\boldsymbol{R}_L {}^L\boldsymbol{b}_1 - \boldsymbol{R}_L {}^L\boldsymbol{b}_2}{||{}^L\boldsymbol{b}_1 - {}^L\boldsymbol{b}_2||} + \lambda_2 \frac{\boldsymbol{R}_L {}^L\boldsymbol{b}_1 - \boldsymbol{R}_L {}^L\boldsymbol{b}_3}{||{}^L\boldsymbol{b}_1 - {}^L\boldsymbol{b}_3||} \\ \bar{\boldsymbol{f}}_2 = -\lambda_1 \frac{\boldsymbol{R}_L {}^L\boldsymbol{b}_1 - \boldsymbol{R}_L {}^L\boldsymbol{b}_2}{||{}^L\boldsymbol{b}_1 - {}^L\boldsymbol{b}_2||} + \lambda_3 \frac{\boldsymbol{R}_L {}^L\boldsymbol{b}_2 - \boldsymbol{R}_L {}^L\boldsymbol{b}_3}{||{}^L\boldsymbol{b}_2 - {}^L\boldsymbol{b}_3||} \\ \bar{\boldsymbol{f}}_3 = -\lambda_2 \frac{\boldsymbol{R}_L {}^L\boldsymbol{b}_1 - \boldsymbol{R}_L {}^L\boldsymbol{b}_3}{||{}^L\boldsymbol{b}_1 - {}^L\boldsymbol{b}_3||} - \lambda_3 \frac{\boldsymbol{R}_L {}^L\boldsymbol{b}_2 - \boldsymbol{R}_L {}^L\boldsymbol{b}_3}{||{}^L\boldsymbol{b}_2 - {}^L\boldsymbol{b}_3||}. \end{cases} \tag{22}$$

Hence, we write the left-hand side of (21) as:

$$\begin{aligned} \bar{\boldsymbol{f}}_1^{\top} \bar{\boldsymbol{R}}_L {}^L\boldsymbol{b}_1 - \bar{\boldsymbol{f}}_1^{\top} \boldsymbol{R}_L {}^L\boldsymbol{b}_1 + \bar{\boldsymbol{f}}_2^{\top} \bar{\boldsymbol{R}}_L {}^L\boldsymbol{b}_2 - \bar{\boldsymbol{f}}_2^{\top} \boldsymbol{R}_L {}^L\boldsymbol{b}_2 + \\ + \bar{\boldsymbol{f}}_3^{\top} \bar{\boldsymbol{R}}_L {}^L\boldsymbol{b}_3 - \bar{\boldsymbol{f}}_3^{\top} \boldsymbol{R}_L {}^L\boldsymbol{b}_3, \end{aligned} \tag{23}$$

Substituting (22) in (23) and solving the inner products, we obtain:

$$\begin{aligned} (1 - \cos(\psi - \bar{\psi})) \Big[& \frac{\lambda_1}{||{}^L\boldsymbol{b}_1 - {}^L\boldsymbol{b}_2||} \left(b_1^2 + b_2^2 - 2 b_1 b_2 \cos \alpha_1 \right) + \\ & + \frac{\lambda_2}{||{}^L\boldsymbol{b}_1 - {}^L\boldsymbol{b}_3||} \left(b_1^2 + b_3^2 - 2 b_1 b_3 \cos \alpha_2 \right) + \\ & + \frac{\lambda_3}{||{}^L\boldsymbol{b}_2 - {}^L\boldsymbol{b}_3||} \left(b_2^2 + b_3^2 - 2 b_2 b_3 \cos \alpha_3 \right) \Big], \end{aligned} \tag{24}$$

where α_1 is the angle between ${}^L\boldsymbol{b}_1$ and ${}^L\boldsymbol{b}_2$, α_2 is the angle between ${}^L\boldsymbol{b}_1$ and ${}^L\boldsymbol{b}_3$, and α_3 is the angle between ${}^L\boldsymbol{b}_2$ and ${}^L\boldsymbol{b}_3$. Note that $b_i > 0$, being it the length of vector ${}^L\boldsymbol{b}_i$. Since, $\forall \ \psi \neq \bar{\psi}$, $(1 - \cos(\psi - \bar{\psi})) > 0$[3], to prove (23) we just need to study the sign of the other terms. To do so, let us study the sign of the following term, where $i, j, k \in \{1,\ 2,\ 3\}$ are chosen as in the terms in (24):

$$\frac{\lambda_k}{||{}^L\boldsymbol{b}_i - {}^L\boldsymbol{b}_j||} \left(b_i^2 + b_j^2 - 2 b_i b_j \cos \alpha_k \right). \tag{25}$$

First, consider that, $\forall k$, $\lambda_k > 0$ by hypothesis. Hence, it is sufficient to consider the sign of

$$b_i^2 + b_j^2 - 2 b_i b_j \cos \alpha_k. \tag{26}$$

To study the sign of (26), let us add and subtract to it the term $2 b_i b_j$, obtaining:

$$\begin{aligned} & b_i^2 + b_j^2 - 2 b_i b_j \cos \alpha_k + 2 b_i b_j - 2 b_i b_j = \\ & = (b_i - b_j)^2 + 2 b_i b_j (1 - \cos \alpha_k) > 0. \end{aligned} \tag{27}$$

This completes the proof[4] for $N = 3$. For $N \neq 3$ the proof is analogous. The difference is that, for $N > 3$, more terms equal to (25) would appear in (24), and, for $N = 2$, fewer terms.

[3]For the periodicity of the cosine function, the quantity is zero also for $\psi = 2k\pi\bar{\psi}$, $\forall k \in \mathbb{N}$, which, however, corresponds to the same equilibrium configuration of our system.

[4]Actually, all terms in (27) are zero, and so is (24), if ${}^L\boldsymbol{b}_1 = {}^L\boldsymbol{b}_i = ... = {}^L\boldsymbol{b}_N$, namely if all the robots are attached to the same point. We reasonably suppose we can disregard such solutions to problem (13), should they occur.

REFERENCES

[1] K.-K. Oh, M.-C. Park, and H.-S. Ahn, "A survey of multi-agent formation control," *Automatica*, vol. 53, pp. 424–440, 2015.

[2] Y. Liu and R. Bucknall, "A survey of formation control and motion planning of multiple unmanned vehicles," *Robotica*, vol. 36, no. 7, pp. 1019–1047, 2018.

[3] F. E. Schneider and D. Wildermuth, "A potential field based approach to multi robot formation navigation," in *IEEE International Conference on Robotics, Intelligent Systems and Signal Processing, 2003. Proceedings. 2003*, vol. 1, pp. 680–685 vol.1, 2003.

[4] P. K. Wang, "Navigation strategies for multiple autonomous mobile robots moving in formation," *Journal of Robotic Systems*, vol. 8, no. 2, pp. 177–195, 1991.

[5] L. Consolini, F. Morbidi, D. Prattichizzo, and M. Tosques, "Leader–follower formation control of nonholonomic mobile robots with input constraints," *Automatica*, vol. 44, no. 5, pp. 1343–1349, 2008.

[6] K.-H. Tan and M. A. Lewis, "Virtual structures for high-precision cooperative mobile robotic control," in *Proceedings of IEEE/RSJ International Conference on Intelligent Robots and Systems. IROS'96*, vol. 1, pp. 132–139, IEEE, 1996.

[7] T. Balch and R. C. Arkin, "Behavior-based formation control for multirobot teams," *IEEE transactions on robotics and automation*, vol. 14, no. 6, pp. 926–939, 1998.

[8] W. Ren and N. Sorensen, "Distributed coordination architecture for multi-robot formation control," *Robotics and Autonomous Systems*, vol. 56, no. 4, pp. 324–333, 2008.

[9] F. E. Schneider and D. Wildermuth, "A potential field based approach to multi robot formation navigation," in *IEEE International Conference on Robotics, Intelligent Systems and Signal Processing, 2003. Proceedings. 2003*, vol. 1, pp. 680–685, IEEE, 2003.

[10] A. D. Dang, H. M. La, T. Nguyen, and J. Horn, "Formation control for autonomous robots with collision and obstacle avoidance using a rotational and repulsive force–based approach," *International Journal of Advanced Robotic Systems*, vol. 16, no. 3, p. 1729881419847897, 2019.

[11] K. Piemngam, I. Nilkhamhang, and P. Bunnun, "A virtual spring damper method for formation control of the multi omni-directional robots in cooperative transportation," in *2019 11th International Conference on Information Technology and Electrical Engineering (ICITEE)*, pp. 1–6, IEEE, 2019.

[12] M. Tognon, C. Gabellieri, L. Pallottino, and A. Franchi, "Aerial co-manipulation with cables: The role of internal force for equilibria, stability, and passivity," *IEEE Robotics and Automation Letters*, vol. 3, no. 3, pp. 2577–2583, 2018.

[13] C. Gabellieri, M. Tognon, D. Sanalitro, L. Pallottino, and A. Franchi, "A study on force-based collaboration in swarms," *Swarm Intelligence*, vol. 14, no. 1, pp. 57–82, 2020.

[14] R. Stopforth, G. Bright, and R. Harley, "Communication and artificial intelligence systems used for the caesar robot," in *Mobile Robots Navigation*, IntechOpen, 2010.

[15] D. Prattichizzo and J. C. Trinkle, "Grasping," in *Springer handbook of robotics*, pp. 955–988, Springer, 2016.

[16] A. Tagliabue, M. Kamel, S. Verling, R. Siegwart, and J. Nieto, "Collaborative transportation using MAVs via passive force control," in *2017 IEEE International Conference on Robotics and Automation (ICRA)*, (Singapore), pp. 5766–5773, 2016.

[17] F. Augugliaro and R. D'Andrea, "Admittance control for physical human-quadrocopter interaction," in *2013 European Control Conference (ECC)*, pp. 1805–1810, IEEE, 2013.

[18] T. Watanabe and T. Yoshikawa, "Grasping optimization using a required external force set," *IEEE Transactions on Automation Science and Engineering*, vol. 4, no. 1, pp. 52–66, 2007.

[19] T. Yoshikawa, "Virtual truss model for characterization of internal forces for multiple finger grasps," *IEEE Transactions on Robotics and Automation*, vol. 15, no. 5, pp. 941–947, 1999.

[20] R. Horst, P. M. Pardalos, and N. Van Thoai, *Introduction to global optimization*. Springer Science & Business Media, 2000.

[21] J. A. E. Andersson, J. Gillis, G. Horn, J. B. Rawlings, and M. Diehl, "CasADi – A software framework for nonlinear optimization and optimal control," *Mathematical Programming Computation*, vol. 11, no. 1, pp. 1–36, 2019.